An Update to Octopus Perimetry

a report by

Ernst Buerki[1] *and* **Matthias Monhart**[2]

1. Private Practitioner, Thun, Switzerland; 2. Product Specialist, Perimetry, Haag-Streit AG

DOI: 10.17925/EOR.2007.00.00.20

How to Define Clusters of Test Locations

Many approaches to the detection and quantitative assessment of local visual defects are described in literature relating to this subject. There is evidence that in normal as well as in pathological visual fields, test locations are relative to one another.[1] Since the threshold in single test locations is highly influenced by fluctuation,[2] grouping of test locations (so-called clustering) is a means of reducing the magnitude of fluctuation. In the assessment of visual fields, judging neighbouring test locations with slightly reduced sensitivity as clusters is considered a valid procedure for the recognition of abnormality, while single test locations at a defect level of eight decibels (dB) are considered to result from normal fluctuation.[3] Local changes are thus identified more easily if they are all part of the investigated cluster of test locations.

Correlations Between Test Locations

In 1982, Wirtschafter et al.[4] gave a first analysis of correlation between test locations. They projected the test locations of visual field examinations onto fundus photographs of primate eyes and grouped them into 15 clusters. Asman and Heijl[5] proved that evaluating clusters following the nerve fibre bundles improved glaucoma detection in humans. Their studies resulted in the Glaucoma Hemifield Test (GHT)[6] using 10 clusters. Weber and Ulrich[7] pursued a different approach, analysing the scotoma borders of 159 glaucoma fields and building 21 clusters according to the affected location's course. Other teams[8,9] applied statistical analysis of glaucomatous visual fields for the definition of the clusters. Garway-Heath et al.[10] followed a different path by measuring the angles of visible retinal nerve fibre layer (RNFL) wedges at the optic disc in 1° steps and correlating them with the corresponding visual field defects. Newly available diagnostic methods have been included in the hunt for improved structure–function correlation. Anton et al.,[11] like Gardiner et al.,[12] compared focal visual field defects with the topographical measurements in 36 sectors of the Heidelberg retina tomograph (HRT) result. Buerki et al.[13] decided to choose a procedure similar to the polar representation at the optic disc. He superimposed the Octopus program G test locations onto a nerve fibre image and followed the corresponding nerve fibres back to the optic disc. Test locations with an exit-angle difference of no more than 5° were grouped to build 22 small clusters. Practical evaluation of the 22 clusters (see *Figure 1a*), which consisted of two test locations, showed that the reduction of fluctuation was not satisfactory. As a consequence, the 22 small clusters were joined to form 10 larger clusters (see *Figure 1b*). These clusters served as starting points for all further computations. Due to the course of the nerve fibres, the clusters do not mirror one another along the horizontal axis.

Quantification of Diffuse and Local Loss

In 1989, Bebie et al.[14] introduced the cumulative defect curve, enabling a simple differentiation between diffuse and local visual field loss (see *Figure 2a*). However, the amount of local and diffuse loss was not calculated. Based

Figure 1a: The Initial 22 Small Clusters

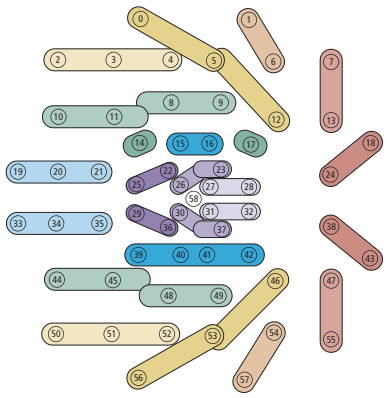

Figure 1b: The Final 10 Clusters for the Octopus G Program

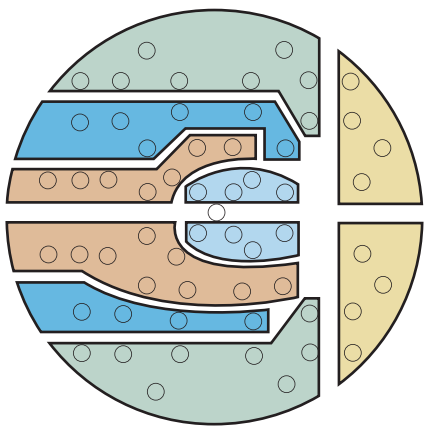

on prior studies evaluating the cumulative defect curve,[15–17] we know that the first third of the curve is spared from increased fluctuation in the initial phase of glaucoma. A diffuse loss can thus be estimated. Heijl suggested the seventh rank (of 74 test locations); Fankhauser et al. suggested ranks 18–19 (of 59 test locations). Following Zulauf's publication on the influence of false-positives[17] and statistical analysis of numerous visual fields, we decided on the average of ranks 12–16 (represented by the arrow in *Figure 2a*), as using the average of a number of ranks rather than relying on a single rank is more resistant to accidental variability. The diffuse defect (DD) can be shown in the cumulative defect curve in two ways: first, as a difference in height of the individual curve compared with the 50th percentile of normality in ranks 12–16 (arrow in *Figure 2a*) and second, as the area between the original 50th percentile and the same curve shifted to match the individual defect curve in ranks 12–16. The dashed area quantifies the diffuse loss in the entire visual field (see *Figure 2b*). It needs to be clarified that DD can only be estimated. Henson et al.[18] showed that in early glaucoma even the first 10 ranks show reduced sensitivity and thus the calculation of DD. Asman[19] further pointed out that the volume of local

Figure 2a: Cumulative Defect Curve

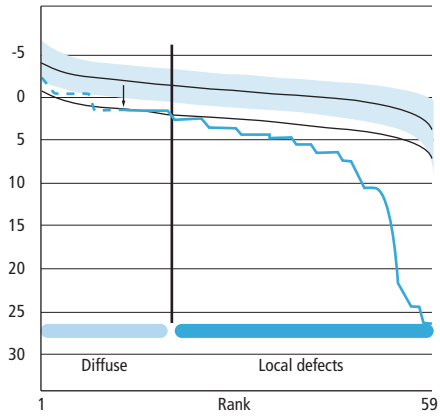

Figure 2b: Diffuse Defect

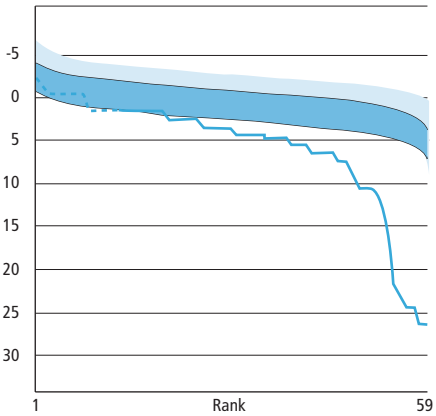

Figure 2c: Abnormal Response Area

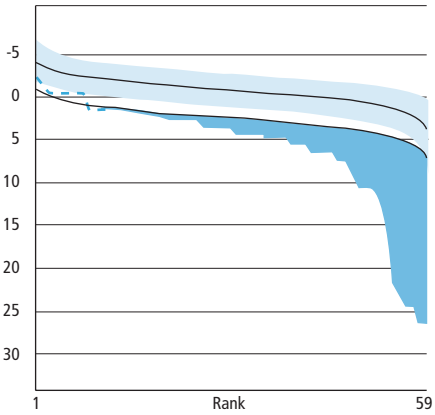

sensitivity reductions correlates with the level of DD. For example, when 20% of test locations are abnormal and the square root of loss variance – sLV/pattern standard deviation (PSD) – is below 10dB, the influence on DD may already be 1dB. Moderate and advanced glaucoma would thus show much more influence on DD. However, Bebie[20] systematically evaluated simulations using the Perisim software[21] and found less influence. *Figure 2c* shows the integration of local loss. This area is defined as the difference between the 50th percentile of the normal defect curve, shifted by DD, and the level of the subject's individual defect curve. While the ranks included in this integrated area do not need to be physical neighbours, they have in common an abnormal response behaviour. Accordingly, this area has been labelled abnormal response area (ARA).[22] This area correlates well with PSD in some cases and has several similarities, including strongly reduced influence of cataract and pupil size, improved recognition of local deviations similar to the pattern deviation and exclusion of the instrument's absolute tolerance – only the difference of response behaviour between an average normal and the tested subject is evaluated; the overall height of sensitivity does not influence this measure. The ARA also has advantages over sLV/PSD, particularly that the influence due to false-positive responses and white scotoma is greatly reduced by the exclusion of the top 20% of ranks.

Looking at these positive aspects, the fact that glaucoma may well have a diffuse component should not be ignored. The influence of false-positives – from trigger-happy subjects – can be quantified using ranks 1–9. Such an index has been stipulated by Zulauf et al.[17] and can be calculated from the cumulative defect curve as a side effect.

Figure 3a: Early Glaucoma in the Right Eye of a 69-year-old Male Subject – Heidelberg Retina Tomography (Left) and Reflection Display (Right)

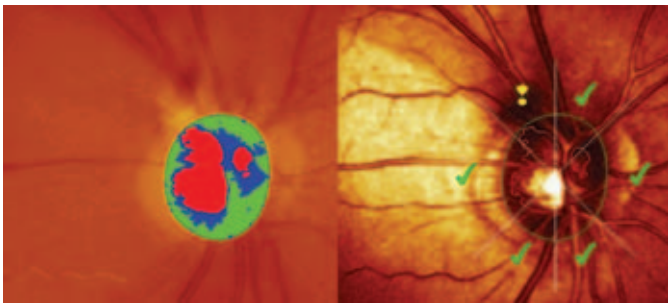

Figure 3b: Probability Plot

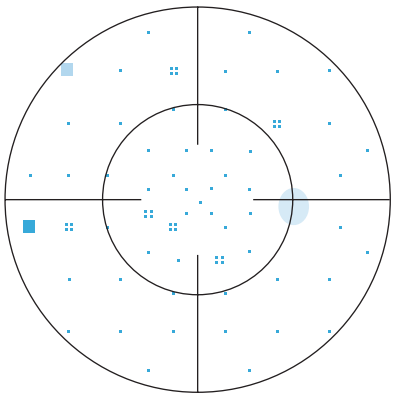

Figure 3c: Cluster Probability

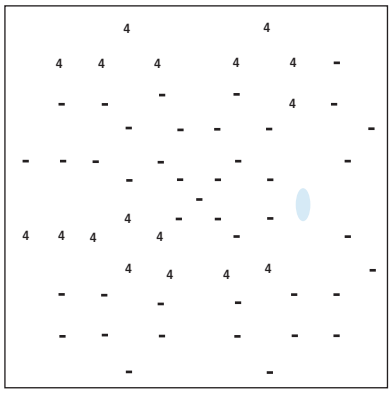

Cluster Analysis

Based on the methods described above and cluster definition, 151 normal subjects have been evaluated to calculate the mean sensitivity and standard deviation for absolute and for shift-corrected (sensitivities after subtraction of DD) defect values. The resulting confidence intervals (CIs) are applied to produce combined probability/defect plots that only display areas outside normal limits. Instead of evaluating every single point, the average cluster defect and probability is displayed. This procedure takes advantage of the reduced fluctuation by clustering and of the choice of evaluating either the absolute sensitivity or the shift-corrected (pattern) deviation.[23] *Figure 3c* is an example of this type of graph. Bold numbers represent a 1% probability level, while the number corresponds to the average defect in dB for the cluster. Normal font represents the 5% probability level. According to the definition of probabilities, on average every 10th normal visual field may have one cluster at the 1% probability level and still belong to a normal subject.

Figure 3d: Polar Graph

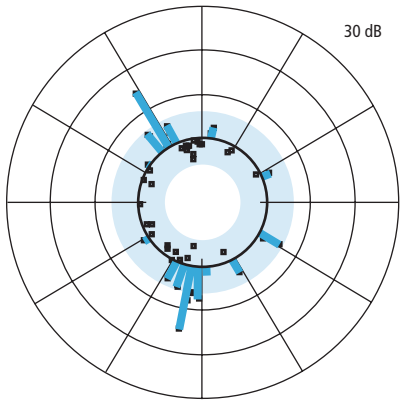

Example

Figure 3a shows two HRT representations. In the topographical image to the left, an excavation is visible on the temporal upper side. The reflection graph to the right shows a visible nerve fibre bundle defect in the same location. The probability plot (see *Figure 3b*) in the G pattern visual field identifies the nasal step and additionally shows a defect in the superior nasal quadrant of the visual field. However, the judgement of the extent and significance of this defect is much more easy to recognise in the cluster analysis in *Figure 3c*. Finally, a bridge between structure and function is given by the polar graph (*Figure 3d*), showing the defect depth in the orientation and position on the optic disc. ■

Availability of the Octopus Field Analysis Software

Octopus Field Analysis software, by Haag-Streit AG, Switzerland is available free of charge for a limited time-trial for evaluation of Octopus G pattern visual fields. Contact the author at matthias.monhart@haag-streit.ch

1. Heijl A, et al., Inter-point correlations of deviation of threshold values in normally and glaucomatous visual fields, *Perimetry Updates*, Amsterdam: Kugler Publications, 1988–89;177–83.
2. Flammer J, Drance SM, Zulauf M, Differential light threshold. Short and long term fluctuation in patients with glaucoma, normally control, and patients with suspected glaucoma, *Arch Ophthalmol*, 1984;102(5):704–6.
3. Chauhan BC, Henson DB, Hobley AJ, Cluster analysis in visual field quantification, *Doc Ophthalmol*, 1988;69(1):25–39.
4. Wirtschafter JD, Becker WL, Howe JD, Younge BR, Glaucoma visual field analysis by computed profiles of nerve fiber function in optic disc second gate, *Ophthalmology*, 1982;89:255–67.
5. Asman P, Heijl A, Spatial correlations in cluster analysis for detection of glaucomatous field loss, *Perimetry Updates*, Amsterdam: Kugler Publications, 1990–91;317–18.
6. Asman P, Heijl A, Glaucoma hemifield test, *Arch Ophthalmol*, 1992;110:812–19.
7. Weber J, Ulrich H, A perimetrc nerve fiber bundle map, *Int Ophthalmology*, 1991;15:193–200.
8. Suzuki Y, Araie M, Ohashi Y, Sectorisation of the central 30° visual field in glaucoma, *Ophthalmology*, 1993;100:69–75.
9. Mandava S, et al., An evaluation of cluster into the glaucomatous visual field, *Amer J Ophthalmol*, 1993;116: 684–91.
10 Garway Heath DF, et al., Mapping the visual field on the optic disc in normal tension glaucoma, *Ophthalmology*, 2000;107:1809–15.
11. Anton A, et al., Mapping structural to functional damage in glaucoma with standard automated perimetry and confocal lasers ophthalmoscopy, *Am J Ophthalmol*, 1998;125:435–46.
12. Gardiner SK, et al., Evaluation of the structure function relationship in glaucoma, *Invest Ophthalmol Vis Sci*, 2005;46:3712–17.
13. Buerki E, Update Octopus perimetrie – Die Polardarstellung der Gesichtsfelddaten, *Ophta*, 2006:7;9–12.
14. Bebie H, Flammer J, Bebie TH, The cumulative defect curve: separation of diffuse and vague components of visual field damage, *Graefes Arch Clin Exp Ophthalmol*, 1989;227:9–12.
15. Heijl A, et al., A package for the statistical analysis of visual fields, *Doc Ophthalmol Proc Series*, 1987;49:153–68.
16. Funkhouser A, Flammer J, et al., A comparison of five methods for estimating general glaucomatous visual field depression, *Graefes Arch Clin Exp Ophthalmol*, 1992;230:101–6.
17. Zulauf M, Becht C, Bernoulli D, False positive peak of the Bebie curve as a reliability parameter, *Perimetry Updates*, Amsterdam: Kugler Publications, 1996–97;185–90.
18. Henson DB, et al., Diffuse loss of sensitivity in early glaucoma, *Invest Ophthalmol Vis Sci*, 1999;40:3147–51.
19. Asman P, Game JM, Heijl A, Appearance of the pattern deviation map as a function of change in area of localised field loss, *Invest Ophthalmol Vis Sci*, 2004;45:3099–3106.
20. Bebie H, personal report.
21. Fankhauser F, et al., Simulation in perimetry – program Perisim 2000, *Ophthalmologica*, 2005;219(3):123–8.
22. Monhart M, Buerki E, Bebie H, Palmowski-Wolfe A, Calculation of the abnormal response area as an indicator of visual field changes, *Invest Ophthalmol Vis Sci*, 2006;47:E-Abstract 3982.
23. Wild JM, et al., The interpretation of the differential threshold into the central visual field, *Doc Ophthalmol*, 1986;28;62(2):191–202.